Crystallization of LiNbO3

Subjects: Materials Science, Ceramics | Chemistry, Inorganic & Nuclear | Physics, Applied

Contributor: Kunfeng Chen

Due to its piezoelectric, ferroelectric, nonlinear optics, and pyroelectric properties, LiNbO3 crystal has found its wide applications in surface acoustic wave (SAW) devices, optical waveguides, optical modulators, and second-harmonic generators (SHG). LiNbO3 crystallized as R3c space group below Curie temperature shows spontaneous polarization that leads to its ferroelectric and piezoelectric properties. Physical and chemical characteristics of LiNbO3 are mainly determined by Li/Nb ratio, impurity cations, vacancies in a cation sublattice. Different sizes of LiNbO3 ranging from nanoscale and microscale to bulk size have been synthesized by solid state method, hydrothermal/solvothermal method, Czochralski (Cz) growth method, etc. Most basic and applied studies of LiNbO3 focus on its bulk single crystal.

Keywords: LiNbO3 ; crystal growth ; piezoelectric property ; optical property

1. Crystal and Defect Structures of $LiNbO_3$

Crystal structure of $LiNbO_3$ can be described as hexagonal unit cells (**Figure 1**a) or rhombohedral unit cells [1][2]. In stoichiometric $LiNbO_3$, along c row direction, the O octahedral interstitials are filled by Li ions (one-third), Nb ions (one-third), and empty (one-third), forming –Li–Nb–□–Li–Nb– sequence [3][4][5]. Much experimental and simulation effort have been made in the past in order to understand the defect structure in LN crystal [6]. Several defect models have been constructed—i.e., oxygen vacancy model, niobium vacancy model ($[Li_{1-5x}Nb_{5x}][Nb_{1-4x}V_{4x}]O_3$), and lithium vacancy model ($[Li_{1-5x}V_{4x}Nb_x]NbO_3$) [3][4][5]. Congruent $LiNbO_3$ crystals were grown with $LiCO_3$ and Nb_2O_5 as starting materials, which contain a high concentration of Nb anti-sites (Nb_{Li}^{4+}) and Li vacancies (V_{Li}^{-}) (**Figure 1**a(ii)) [7]. Owing to atomic radius differences between Nb and Li, it forbids Li replacement in a Nb site. Thus, the composition deviates from stoichiometric only toward the Nb-rich side [8][9]. The Li vacancy model is mostly accepted nowadays thanks to a great number of investigations, some of them very important and performed in the 1990s. This is given in detail in [6]. Since these defects are charged, further defects with counter charges are required in order to guarantee overall charge neutrality [9]. Thus, for energetic reasons, complex ionic complexes and spaced clusters are present as shown in **Figure 1**b [2]. However, debate still prevails on the available models on defect clusters. The understanding and control of $LiNbO_3$ intrinsic and extrinsic defects during crystallization and operational process is important for specific applications.

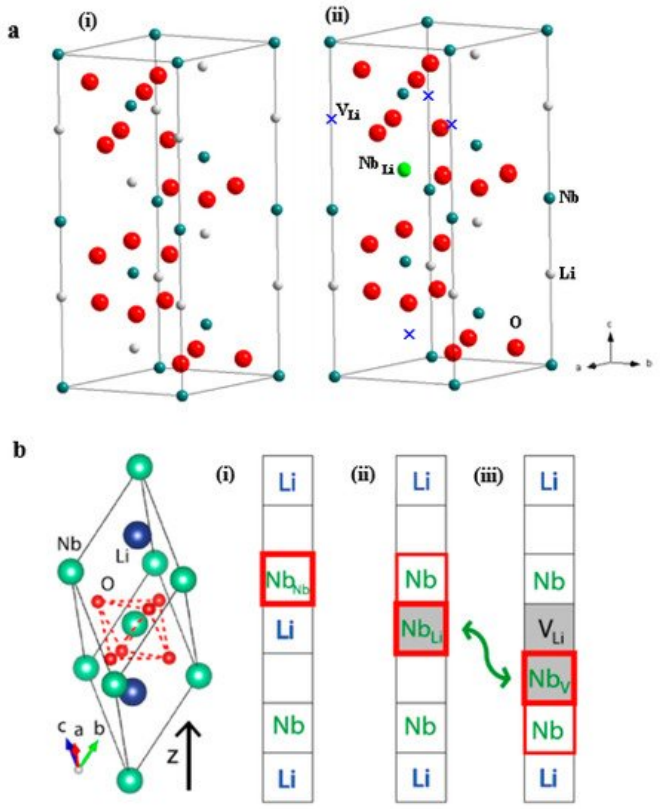

Figure 1. (**a**) Crystal structures of stoichiometric $LiNbO_3$ (i) and congruent LN with anti-site Nb_{Li}^{4+} and V_{Li}^{-} defects (ii) [8]; (**b**) Free and defect-bound (bi)polarons in $LiNbO_3$ [2].

2. Crystallization of $LiNbO_3$

According to binary phase diagram, $LiNbO_3$ has a large solid solution range, which can exist and be stable on Li composition from 46.5 mol% to 50 mol% (**Figure 2**). The liquid–solid curve reveals a diffuse maximum at approximately 48.6% Li_2O [10]. With exceeding composition range, the secondary $LiNb_3O_8$ and Li_3NbO_4 phases can be created. The binary phase diagram can be determined by measuring XRD of different samples along solid lines. However, it is also needed to probe precise composition range, because $LiNbO_3$'s bulk properties are composition dependent [11].

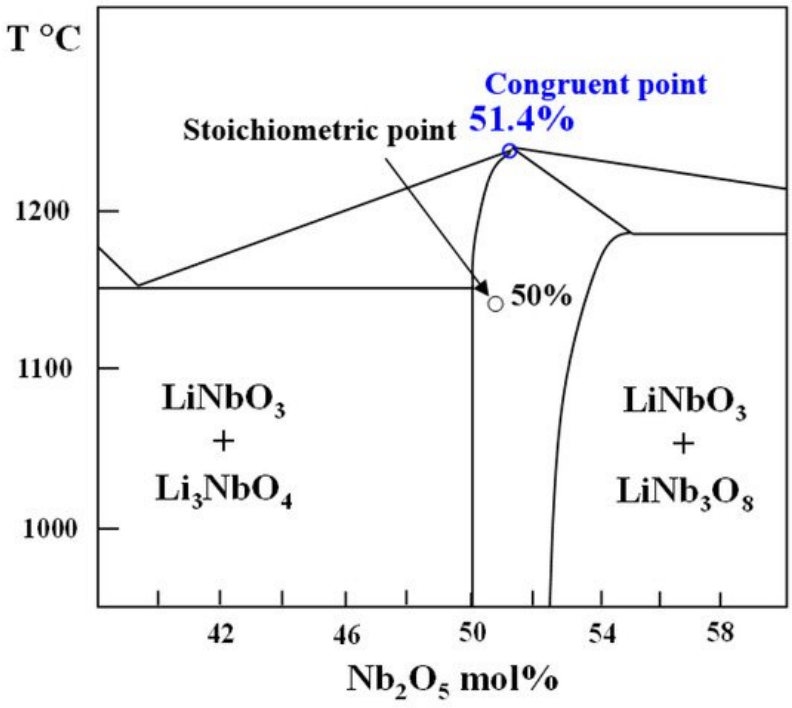

Figure 2. Schematic equilibrium phase diagram of binary system of Li_2O and Nb_2O_5 m in the vicinity of $LiNbO_3$.

$LiNbO_3$ polycrystalline can be grown by solid-state reaction, sol–gel, hydrothermal, vapor phase methods. The crystallization method of $LiNbO_3$ single crystal includes Cz, Bridgeman, high-temperature top-seeded solution growth. Cz

method is the current mainstream technology for growing bulk $LiNbO_3$ single crystal [12][13][14]. With $LiNbO_3$ polycrystalline as starting materials, the Cz crystal growth is often controlled by the pulling/rotation rate and heater power [15][16]. The growth of $LiNbO_3$ crystal was affected by various factors together, such as the ratio of raw materials, quality of seed crystal, temperature gradient, growth parameters, etc. [10]. In reality, the Li evaporation at high temperature is hard to be eliminated, which results in the segregation of Li content inside the as-grown crystal. Congruent $LiNbO_3$ with good compositional uniformity can be formed with Li content can range from 47 to 50 mol%. Nearly stoichiometric $LiNbO_3$ composition can be achieved by more elaborate growth processes.

A slower pulling rate is helpful to obtain a crystal with less internal stress and high quality. **Table 1** shows pulling rate and rotation rate [12][13][14][15][16]. Recently, 6-inch $LiNbO_3$ crystals have been grown with a rotation rate of 5~10 rpm, and the pulling rate of 1–2 mm/h [12]. The obtained 6-inch $LiNbO_3$ crystal shows good homogeneity with the absolute deviation of Curie temperature ≤1.3 °C. In addition, fast growth rate can lead to low-cost $LiNbO_3$ crystal, which is important for industry production. Thus, under the premise of ensuring quality, fast pulling rate is also demanded.

Table 1. Growth parameters of $LiNbO_3$ reported in literatures.

Pulling Rate (mm/h)	Rotation Rate (rpm)	Size ϕ × l (mm)	Li Content (mol%/cm)	Ref.
1–2	5–10	153 × 110	$\Delta[Li_2O] \approx 0.001$	[12]
0.3–3	20–35	8 × 10	-	[13]
1	7	30 × 50	-	[14]
0.4–1.5	10–30	50 × 30	$\Delta[Li_2O] < 0.005$	[15]
1–2.5	10–25	80 × 60	$\Delta[Li_2O] < 0.02$	[16]
2.8–4.0	3–10	100 × 80	$\Delta[Li_2O] < 0.002$	[8]

3. Composition Characterizations of $LiNbO_3$

The performances of $LiNbO_3$ are most depend upon their chemical composition. Therefore, the development of the precise analysis method to detect the chemical composition (Li content) of $LiNbO_3$ is very important. **Table 2** shows available testing methods for determine Li content of $LiNbO_3$, for example, X-ray diffraction (XRD), Raman spectroscopy (RS), UV–vis diffuse reflectance (DR), and differential thermal analysis (DTA) [17][18][19][20][21][22].

Table 2. Testing method of Li composition for $LiNbO_3$.

Testing Method	Advantages	Disadvantages
Raman scattering method	Raman systems have become cheaper and easier to use	The use of a correct configuration of the detection and excitation polarizers (in the case of single crystals)
Curie temperature	Linearly with Li/[Li + Nb] ratio Reliable and sufficient sensitivity for composition	High Curie temperature close to the melting point
UV absorption edge	Convenient and accurate way for determining the composition	Nonlinear relationship Accuracy is governed by the wavelength calibration Doping compound will deteriorate the accuracy
Refractive indices	Function of wavelength and stoichiometry	Nonlinear relationship
Birefringence	Approximately linear correspondence between Li content and birefringence	The nonlinear relationships dominated by the wavelength

In Raman spectroscopy, the Li content can be calculated according to the linewidth (Γ) at 876 cm^{-1} [23][24][25].

$$C_{Li} = 53.29–0.1837\Gamma \quad (1)$$

The Li content of $LiNbO_3$ can be also calculated via measuring Curie temperature

$$C_{Li} = 17.37 + 0.02725T_c \quad (2)$$

where T_c is Curie temperature in °C. Curie temperature is the temperature at which $LiNbO_3$ tends to lose its ferroelectric properties. When use above reported characterizations, the applicability and calibration method need to be concerned.

Some indirect optical and non-optical methods for the determination of the chemical composition of LN single crystals can be referred to [6].

References

1. Kong, Y.; Bo, F.; Wang, W.; Zheng, D.; Liu, H.; Zhang, G.; Rupp, R.; Xu, J. Recent progress in lithium niobate: Optical damage, defect simulation, and on-chip devices. Adv. Mater. 2020, 32, 1806452.
2. Schmidt, F.; Kozub, A.L.; Biktagirov, T.; Eigner, C.; Silberhorn, C.; Schindlmayr, A.; Schmidt, W.G.; Gerstmann, U. Free and defect-bound (bi)polarons in LiNbO3: Atomic structure and spectroscopic signatures from ab initio calculations. Phys. Rev. Res. 2020, 2, 043002.
3. Zotov, N.; Boysen, H.; Frey, F.; Metzger, T.; Born, E. Cation substitution models of congruent LiNbO3 investigated by X-ray and neutron powder diffraction. J. Phys. Chem. Solids 1994, 55, 145–152.
4. Kim, S.; Gopalan, V. Domain reversal and nonstoichiometry in lithium tantalate. J. Appl. Phys. 2001, 90, 2949–2963.
5. Teplyakova, N.A.; Sidorov, N.V.; Palatnikov, M.N. Determination of stoichiometry, concentration of OH groups, and point defects in lithium niobate crystals from their IR absorption spectra. Opt. Spectrosc. 2020, 128, 1131–1137.
6. Sánchez-Dena, O.; Fierro-Ruiz, C.D.; Villalobos-Mendoza, S.D.; Carrillo Flores, D.M.; Elizalde-Galindo, J.T.; Farías, R. Lithium niobate single crystals and powders reviewed—Part I. Crystals 2020, 10, 973.
7. Palatnikov, M.N.; Biryukova, I.V.; Masloboeva, S.M.; Makarova, O.V.; Kravchenko, O.E.; Yanichev, A.A.; Sidorovet, N.V. Structure and optical homogeneity of LiNbO3 ⟨Mg⟩ crystals grown from different charges. Inorg. Mater. 2013, 49, 715.
8. Chen, K.; Li, Y.; Peng, C.; Lu, Z.; Luo, X.; Xue, D. Microstructure and defect characteristics of lithium niobate with different Li concentrations. Inorg. Chem. Front. 2021, 8, 4006–4013.
9. Kohler, T.; Mehner, E.; Hanzig, J.; Gärtner, G.; Funke, C.; Joseph, Y.; Leisegang, T.; Stöcker, H.; Meyer, D.C. Kinetics of the hydrogen defect in congruent LiMO3. J. Mater. Chem. C 2021, 9, 2350–2367.
10. Reisman, A.; Holtzberg, F. Heterogeneous Equilibria in the Systems Li2O-, Ag2O-Nb2O5 and Oxide-Models. J. Am. Chem. Soc. 1958, 80, 6503–6507.
11. Sanna, S.; Schmidt, W. LiNbO3 surfaces from a microscopic perspective. J. Phys. Condens. Matter 2017, 29, 413001.
12. Wang, S.; Ji, C.; Dai, P.; Shen, L.; Bao, N. The growth and characterization of six inch lithium niobate crystals with high homogeneity. CrystEngComm 2020, 22, 794–801.
13. Zhang, X.; Liang, G.; Xu, Z. Defect structure and holographic storage properties of LiNbO3:Zr:Fe:Cu crystals with various Li/Nb ratios. Opt. Mater. 2019, 96, 109318.
14. Kong, T.; Liang, P.; Liu, H.; Zheng, D.; Liu, S.; Chen, S.; Kong, Y.; Xu, J. Study on the Growth and Optical Damage Resistance of Ternary Congruent Mg-doped LiNbO3 Crystal. J. Synthetic Crystals 2018, 8, 1507–1511.
15. Zheng, Y.; Kong, H.; Chen, H.; Xin, J.; Lu, Z.; Shi, E. Growth and ferroelectric domain control of homogeneous MgO-doped near-stoichiometric lithium niobate single crystals by melt-supplying technique. J. Cryst. Growth 2008, 310, 1966–1970.
16. Xu, B.; Xia, Z.; Li, C.; Cui, K.; Ye, S.; Zhang, C. Growth and Measurement Method of Optics-grade and Large Diameter Lithium Niobate Crystals. J. Synthetic Crystals 2002, 5, 516–519.
17. Zhi, Y.; Zhu, Y.; Pan, W.; Tianet, K. Optical method to determine the composition of lithium niobate crystals by digital holography. Appl. Opt. 2020, 59, 315.
18. Sánchez-Dena, O.; Villagómez, C.J.; Fierro-Ruíz, C.D.; Padilla-Robles, A.S.; Farías, R.; Vigueras-Santiago, E.; Hernández-López, S.; Reyes-Esqueda, J.A. Determination of the chemical composition of lithium niobate powders. Crystals 2019, 9, 340.
19. Kokanyan, N.; Chapron, D.; Fontana, M. Temperature dependence of Raman scattering and anharmonic properties in LiNbO3. Appl. Phys. A 2014, 117, 1147.
20. Redfield, D.; Burke, W.J. Optical absorption edge of LiNbO3. J. Appl. Phys. 1974, 45, 4566.
21. Hu, L.J.; Chang, Y.H.; Chang, C.S. Raman and NMR study in MgO-doped LiNbO3 crystal, Mod. Phys. Lett. B 1991, 5, 789–797.
22. Fontana, M.D.; Bourson, P. Microstructure and defects probed by Raman spectroscopy in lithium niobate crystals and devices. Appl. Phys. Rev. 2015, 2, 040602.
23. Margueron, S.; Margueron, S.; Bartasyte, A.; Glazer, A.M.; Simon, E.; Hlinka, J.; Gregora, I.; Gleize, J. Resolved E-symmetry zone-centre phonons in LiTaO3 and LiNbO3. J. Appl. Phys. 2012, 111, 104105.

24. Wohlecke, M.; Corradi, G.; Betzler, K. Optical methods to characterise the composition and homogeneity of lithium niobate single crystals. Appl. Phys. B 1996, 63, 323–330.
25. Schlarb, U.; Klauer, S.; Wesselmann, M.; Betzler, K.; Wöhlecke, M. Determination of the Li/Nb ratio in lithium niobate by means of birefringence and Raman measurements. Appl. Phys. A 1993, 56, 311–315.